

Electronic Supplementary Information

Stabilization of Ruthenium Nanoparticles over NiV-LDH Surface for Enhanced Electrochemical Water Splitting: An Oxygen Vacancy Approach

**Arun Karmakar, †‡ Kannimuthu Karthick, †‡ Selvasundarasekar Sam Sankar, †‡
Sangeetha Kumaravel, †‡ Ragunath Madhu, †‡ Krishnendu Bera, †‡ Hariharan N
Dhandapani, †‡ Sreenivasan Nagappan, †‡ Palanichamy Murugan^{†@*} and Subrata
Kundu †‡***

[†]*Academy of Scientific and Innovative Research (AcSIR), Ghaziabad-201002, India.*

[‡]*Electrochemical Process Engineering (EPE) Division, CSIR-Central Electrochemical
Research Institute (CECRI), Karaikudi-630003, Tamil Nadu, India.*

[@]*Electrochemical Power Source (ECPS) Division, CSIR-Central Electrochemical Research
Institute (CECRI), Karaikudi-630003, Tamil Nadu, India.*

*To whom correspondence should be addressed, *E-mail:* skundu@cecri.res.in;
kundu.subrata@gmail.com, murugan@cecri.res.in, Phone/Fax: (+ 91) 4565-241487.

This file contains 31 pages in which the details of reagents, methods of synthesis, electrochemical characterizations, electrochemical results, characterizations like SEM, FE-SEM and post OER and post HER SEM, FE-SEM, HR-TEM and XPS results are provided.

Number of Figure: 21

Number of Table: 1

| Figures | Subject of the Figure | Page number |
|----------------|--|--------------------|
| S1 | Low to high magnified FE-SEM images of NiV-LDH materials revealing the sheet-like morphology. | S8 |
| S2 | Low to high magnified FE-SEM images of Ru@NiV-LDH materials revealing the sheet like morphology. | S9 |
| S3 | EDS spectrum of NiV-LDH with corresponding quantification of all the expected elements. | S10 |
| S4 | EDS spectrum of NiV-LDH with corresponding quantification of all the expected elements | S11 |
| S5 | Low to high magnified FE-SEM images of NiV-LDH(Vo) revealing sheet like structure was retained even after vacancy creation through the NaBH ₄ reduction under hydrothermal condition and EDS spectrum obtained in FE-SEM mode. | S12 |
| S6 | Combined XPS survey spectrum of NiV-LDH and Ru@NiV-LDH. | S13 |
| S7 | DFT optimized structure of Ru ₆ , Ru ₈ and Ru ₁₄ clusters. | S14 |
| S8 | (a) Ball and stick model of optimized structure of monolayer of Ni ₅ /6V ₁ /6(OH) ₂ compound (top view); (b) Ru ₆ cluster deposited on Ni ₅ /6V ₁ /6(OH) ₂ compound, and (c) closer view of (b) to understand bonding between O-Ru atoms. Blue, light grey, red, turquoise blue and white balls represent Ni, V, O, Ru and H atoms, respectively. Dotted black line indicates boundary of supercell. Bond distances are shown in Å. | S15 |
| S9 | (a) Optimized structure of Ru ₆ cluster adsorbed on oxygen deficient surface (b) closer view of the cluster and surface. Blue, light grey, red, turquoise blue and white balls represent Ni, V, O, Ru and H atoms, respectively. Dotted line indicates boundary of supercell. Bond distances are shown in Å. | S16 |
| S10 | (a) Optimized structure of Ru ₆ cluster adsorbed on oxygen deficient surface (b) closer view of the cluster and surface. Blue, light grey, red, turquoise blue and white balls represent Ni, V, O, Ru and H atoms, respectively. Dotted line indicates boundary of supercell. Bond distances are shown in Å. | S17 |
| S11 | LSV polarization curve for Ru@CC obtained at a scan rate of 5 mV/sec in 1 M KOH solution. | S18 |
| S12 | (a-d) are the CVs recorded in a non-faradaic region with increasing scan rate for the | S19 |

| | | |
|------------|--|------------|
| | determination of ECSA from its double layer capacitance taking NiV-LDH, NiV-LDH(Vo), NiVRu-LDH and Ru@NiV-LDH respectively. | |
| S13 | (a), (b) and (c) Reduction surface area of Ru@NiV-LDH, NiV-LDH and NiV-LDH (Vo) respectively. | S21 |
| S14 | Faradaic efficiency plot obtained by plotting the amount of O ₂ produced at different time interval. | S22 |
| S15 | LSV polarization curves for Ru@NiV-LDH materials before and after the AD study. | S23 |
| S16 | LSV polarization curves of NiV-LDH(Vo) and Ru@CC under HER condition. | S24 |
| S17 | EIS analysis of NiV-LDH and Ru@NiV-LDH in HER condition. | S25 |
| S18 | (a-b) CV curves obtained at different scan rate for NiV-LDH and Ru@NiV-LDH respectively; (c) corresponding Cdl plot and (d) ECSA normalized LSV polarization curves. | S26 |
| S19 | XRD pattern of Ru@NiV-LDH before and after the electrolysis. | S27 |
| S20 | Pre and post OER, FE-SEM picture of Ru@NiV-LDH. | S28 |
| S21 | (a-c) low to high magnified Post OER HR-TEM images of Ru@NiV-LDH nanosheets; (d) HAADF area chosen for colour mapping and (e-k) showing the colour mapping results of HAADF+Ni+V, mix, Ni K shell, V K shell, O K shell and C K shell orbitals respectively. | S29 |
| S22 | (a) high resolution XPS spectra of Ni 2p orbitals post OER Ru@NiV-LDH respectively; (b) Ru 3d XPS result; (c) High resolution XPS spectra of V 2p orbital; (d) O 1s orbital XPS spectra. | S30 |
| | References | S31 |

Reagents and Instruments:

Nickel chloride (NiCl₂), Vanadium trichloride (VCl₃), RuCl₃.xH₂O and Sodium borohydride (NaBH₄) were purchased from Sigma-Aldrich and used as received. Sodium carbonate (Na₂CO₃) was purchased from Merck and used as received. Ni foam was procured from Sigma-Aldrich and used after surface cleaning. The electrochemical analyzer AURT-M204 was used for all electrochemical characterizations. Hg/HgO reference electrode (in 1 M KOH), SCE reference electrode (in 0.5 M H₂SO₄) were purchased from CH instruments and

carbon cloth as counter electrode from Alfa-Aesar were used throughout the electrochemical studies. DI water was used throughout entire experiments. The as prepared catalysts with different stoichiometric ratios were characterized with HR-TEM, (Tecnai™ G² TF20) working at an accelerating voltage of 200 kV and by Talos F-200-S with HAADF elemental mapping. Color mapping and Energy Dispersive X-ray Spectroscopy (EDS) analysis were carried out with the FESEM instrument with the images (SUPRA 55VP Carl Zeiss) with a separate EDS detector connected to that instrument. Scanning Electron Microscopy (SEM) analysis was carried with a Hitachi, Japan make model S-3000H instrument having magnification 30X to 300 KX with the accelerating voltage ~ 0.3 to 30 kV. The XRD analysis carried out with a scanning rate of 5° min⁻¹ in the 2θ range 10-90° using a Rigaku X-ray powder diffractometer (XRD) with Cu K_α radiation (λ = 0.154 nm). X-ray photoelectron spectroscopic (XPS) analysis was performed using a Theta Probe AR-XPS system (Thermo Fisher Scientific, UK). ICP-MS analysis was carried by using iCAP RQ from thermoscientific instrument. For ICP analysis, 1 ml of stock solution was taken and evaporate to dryness at 90 °C to remove the water from the sample. Then it was digested by adding aqua regia followed by heating for 1 to 2 minutes. Then the resulted solution was used for analysis by diluting 10 times with water.

Synthesis of NiV-LDH(V_o):

For the typical synthesis, 150 mg of NiV-LDH powder was taken in 100 ml beaker containing 30 mL of DI water subsequently stirred for 15 min to ensured homogeneity of the solution. After that the solution was transferred into 50 mL Teflon lined autoclave followed by addition of 0.11 g of NaBH₄. The whole solution was kept in hydrothermal condition for 6 hours at a temperature of 180 °C. After cooling, solid product was collected by centrifugation. The solid was washed with ethanol water mixture for the five times to remove the sodium ions from the surface.

Computational Methodology:

All results used in this work are obtained by employing plane wave based first principles DFT calculations as implemented in Vienna *Ab initio* Simulation Package (VASP). All atoms are described by projector augmented wave pseudopotential formalism (PAW)¹ and exchange correlations for electron-electron interactions are corrected by generalized gradient approximations (GGA).²The kinetic energy cut-off of 400 eV is used for plane-wave basis sets. O, OH, and OOH species are allowed to adsorb on Ru₈ cluster adsorbed on surface to deduce the chemical reaction co-ordinate diagram. The sufficient vacuum space of 7 - 8 Å is considered to nullify the interaction between the slab and its periodic images. The Brillouin zone is sampled using Gamma centered 5 × 5 k-mesh. All the ions are fully relaxed without considering any symmetry. The iterative relaxation processes are repeated until the absolute force on each ion is converged to in order of 0.01 eV/Å and the energy difference between two ionic steps is converged to 10⁻⁵ eV in all the calculations. Entire calculations are performed by the spin polarized calculations, in which, moments of all transition metal atoms are ferromagnetically aligned.

Initially, the supercell with size of $2\sqrt{3} \times 2\sqrt{3}$ monolayered Ni(OH)₂ compound was modelled and understood the interaction between this surface and Ru clusters. The cell parameter ($a = 3.08$ and $\gamma = 120^\circ$) is taken from our present experiment. Three different sized Ru atomic clusters (Ru₆, Ru₈, and Ru₁₄) are considered for their adsorption onto this surface in order to deduce the consistency of our results. These clusters are deposited onto pristine Ni(OH)₂ surface and the structural and energetics are deduced by performing first principles calculations. The optimized structures of three clusters adsorbed on this surface are shown in Fig. S8 (supporting information). The adsorption energy is obtained from,

$$E_{ad} = E_{clean} + E_{cluster} - E_{adsorbed}$$

where, E_{clean} , E_{cluster} , and E_{adsorbed} are total energies of clean surface, isolated Ru cluster, and cluster adsorbed on the surface, respectively.

❖ **Determination of Surface concentration of various alloys from the redox features of CV:**

- Calculated area associated with the oxidation of Ni^{3+} to Ni^{2+} of **NiV-LDH** = 0.00143 VA

Hence, the associated charge is = $0.00143 \text{VA} / 0.005 \text{Vs}^{-1}$

$$= 0.286 \text{ As}$$

$$= \mathbf{0.286 \text{ C}}$$

Now, the number of electron transferred is = $0.286 \text{ C} / 1.602 \times 10^{-19}$

$$= \mathbf{1.785 \times 10^{17}}$$

Since, the reduction of Ni^{3+} to Ni^{2+} is a single electron transfer reaction, the number electron calculated above is exactly the same as the number of surface-active sites.

Hence, the number of Ni participate in OER is = $\mathbf{1.785 \times 10^{17}}$

Determination of Turnover Frequency (TOF) from OER Current Density TOF in our study was calculated assuming that the surface-active Co atoms that had undergone the redox reaction just before onset of OER only participated in OER electrocatalysis. The corresponding expression is,

$$\text{TOF} = j \times N_A / F \times n \times \Gamma$$

Where, j = current density N_A = Avogadro number F = Faraday constant n = Number of electrons Γ = Surface concentration.

Hence, we have,

$$\text{TOF}_{1.50 \text{ V}} = [(5.37 \times 10^{-4}) (6.023 \times 10^{23})] / [(96485) (4) (1.785 \times 10^{17})]$$

$$= \mathbf{0.00469 \text{ sec}^{-1}}$$

- Calculated area associated with the oxidation of Ni^{3+} to Ni^{2+} of **NiV-LDH(V_o)** = 0.00171 VA

Hence, the associated charge is = $0.00171 \text{ VA} / 0.005 \text{ Vs}^{-1}$

$$= 0.342 \text{ As}$$

$$= \mathbf{0.342 \text{ C}}$$

Now, the number of electron transferred is = $0.342 \text{ C} / 1.602 \times 10^{-19}$

$$= \mathbf{2.13 \times 10^{17}}$$

Since, the oxidation of Ni^{3+} to Ni^{2+} is a single electron transfer reaction, the number electron calculated above is exactly the same as the number of surface-active sites.

Hence, the number of Ni participate in OER is = $\mathbf{2.13 \times 10^{17}}$

Hence,

$$\text{TOF}_{1.50\text{V}} = [(7.6 \times 10^{-4}) (6.023 \times 10^{23})] / [(96485) (4) (2.13 \times 10^{17})]$$

$$= \mathbf{0.00556 \text{ sec}^{-1}}$$

- Calculated area associated with the oxidation of Ni^{3+} to Ni^{2+} of **Ru@NiV-LDH** = 0.00287 VA

Hence, the associated charge is = $0.00287 \text{ VA} / 0.005 \text{ Vs}^{-1}$

$$= 0.574 \text{ As}$$

$$= \mathbf{0.574 \text{ C}}$$

Now, the number of electron transferred is = $0.574 \text{ C} / 1.602 \times 10^{-19}$

$$= \mathbf{3.58 \times 10^{17}}$$

Since, the reduction of Ni^{3+} to Ni^{2+} is a single electron transfer reaction, the number electron calculated above is exactly the same as the number of surface-active sites.

Hence, the number of Ni participate in OER is = $\mathbf{3.58 \times 10^{17}}$

Hence,

$$\text{TOF}_{1.50\text{V}} = [(8.6 \times 10^{-3}) (6.023 \times 10^{23})] / [(96485) (4) (3.58 \times 10^{17})]$$

$$= \mathbf{0.0374 \text{ sec}^{-1}}$$

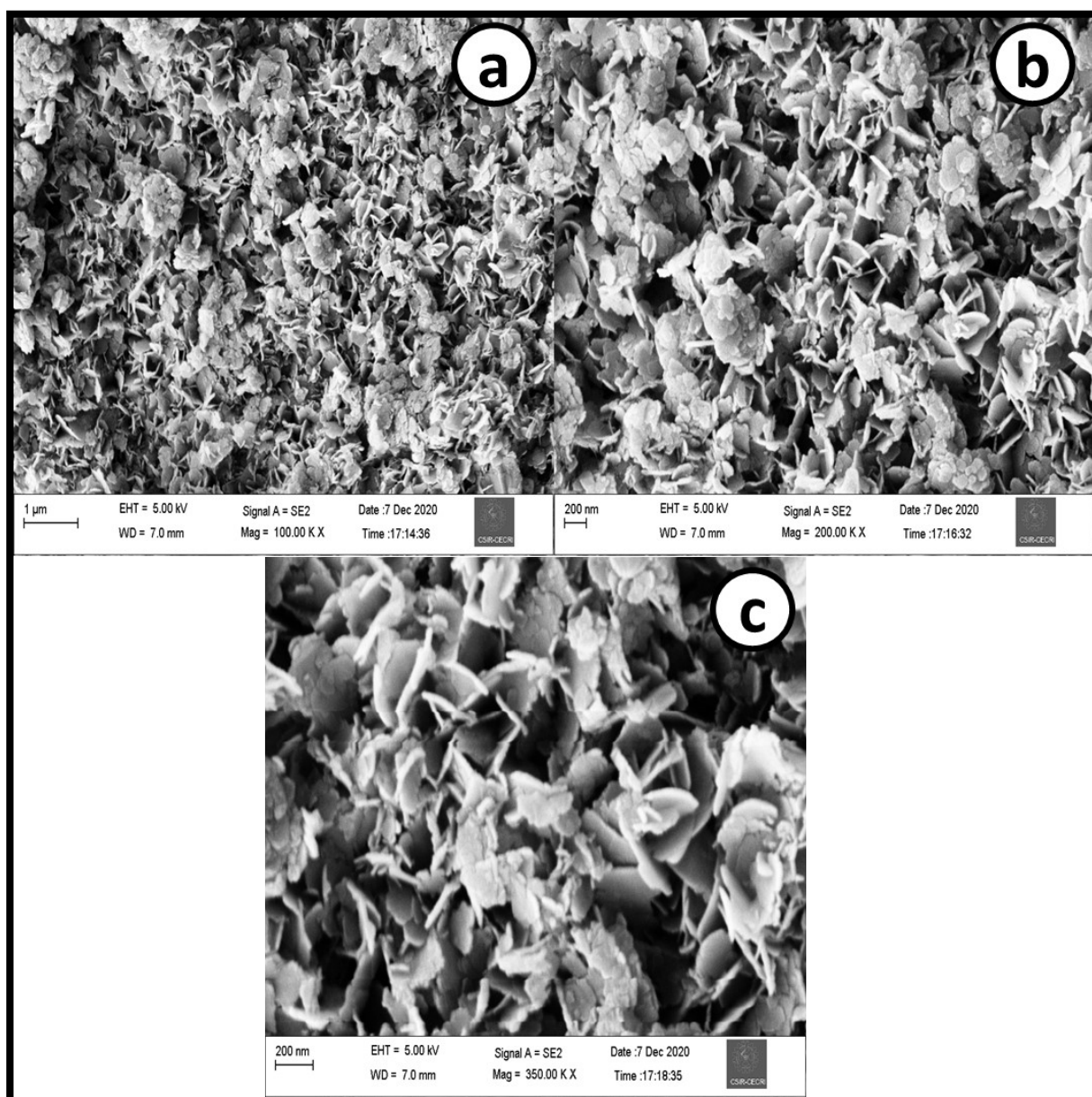


Figure S1: (a-c) low to high magnified FE-SEM images of NiV-LDH materials revealing the sheet-like morphology.

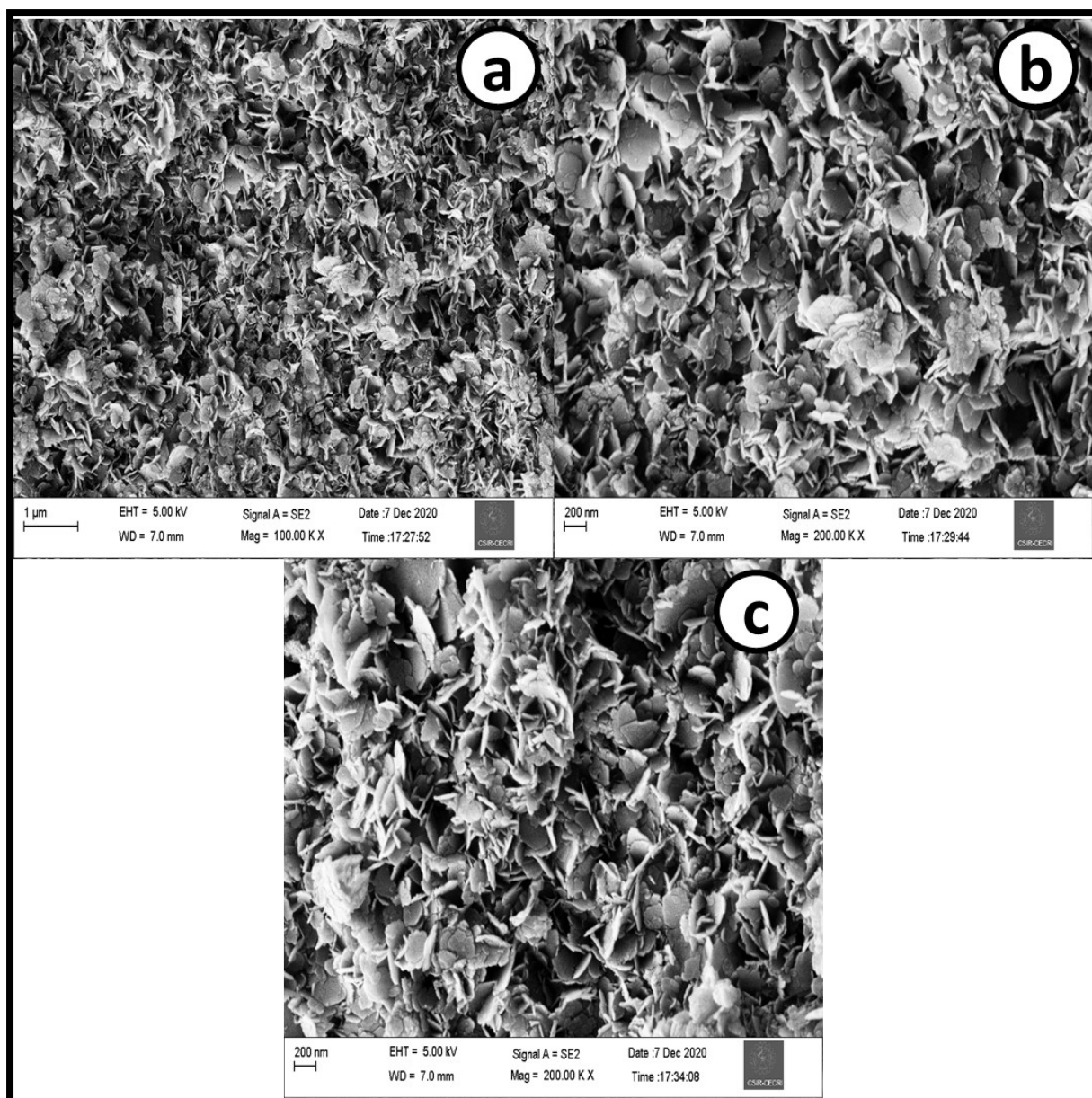


Figure S2: (a-c) low to high magnified FE-SEM images of Ru@NiV-LDH materials revealing the sheet like morphology.

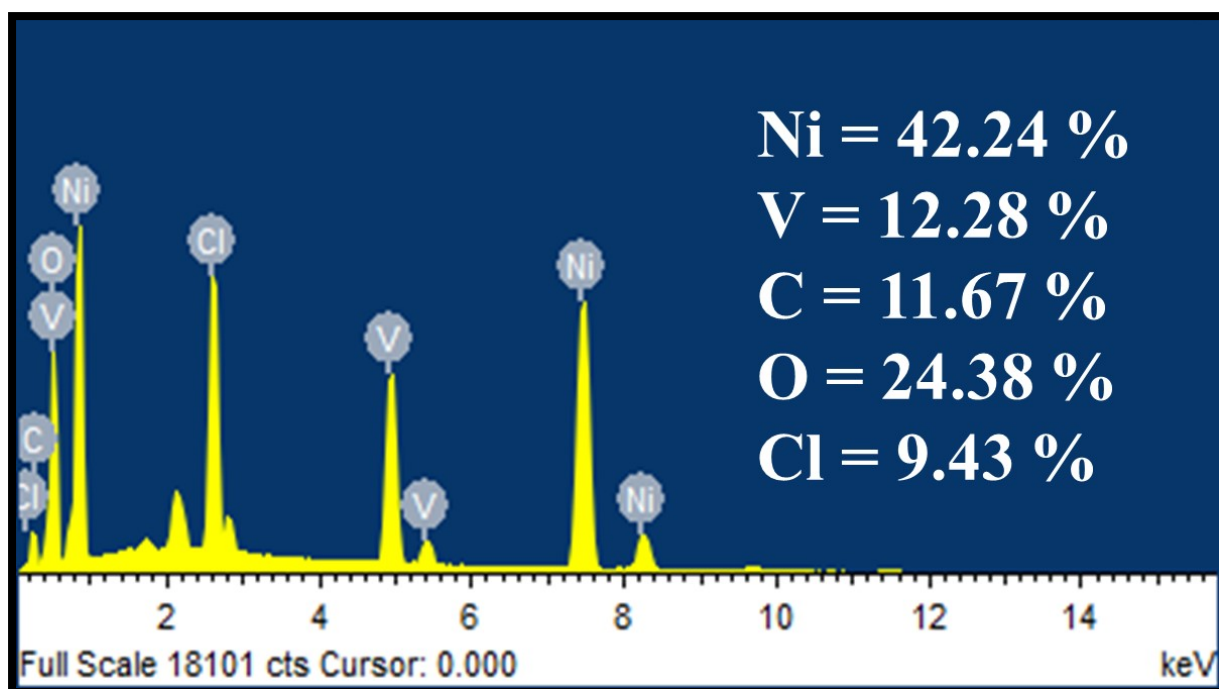


Figure S3: EDS spectrum of NiV-LDH with corresponding quantification of all the expected elements.

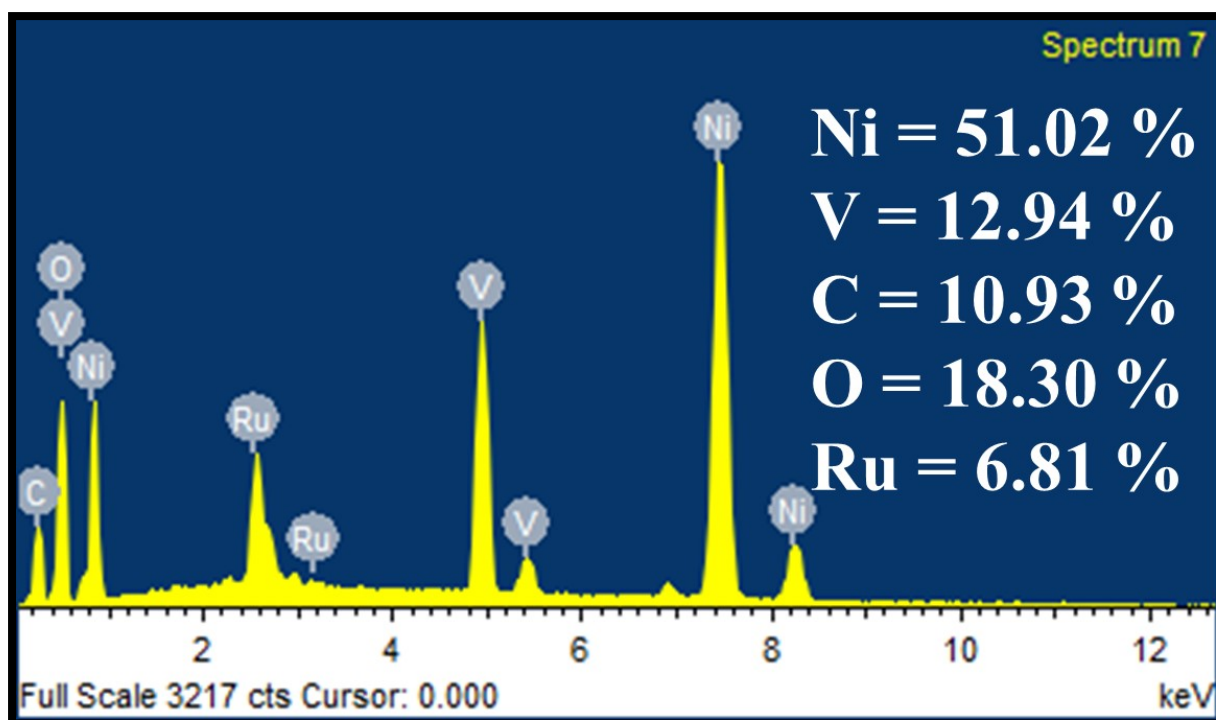


Figure S4: EDS spectrum of Ru@NiV-LDH with corresponding quantification of all the expected elements.

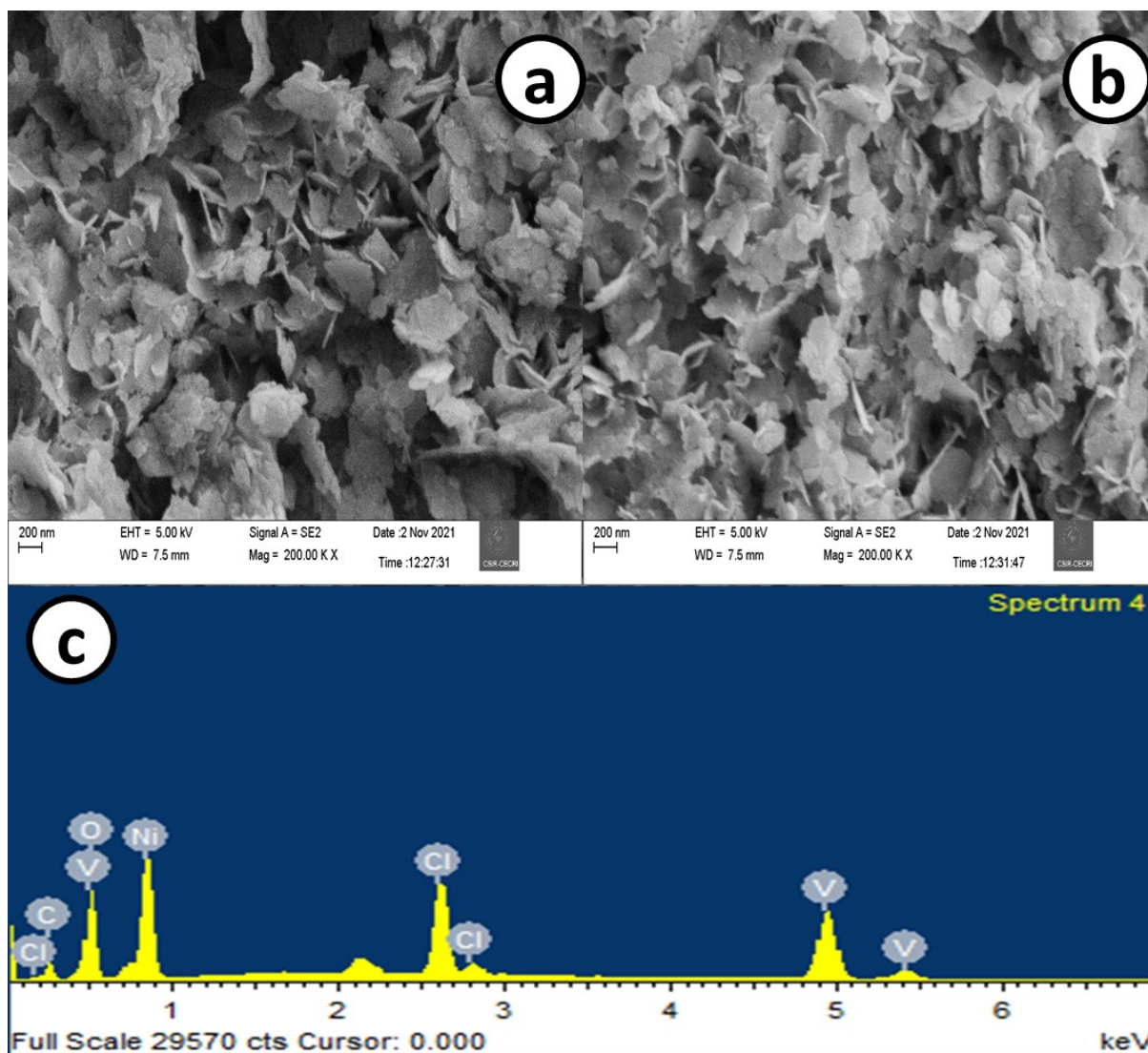


Figure S5: (a-b) low to high magnified FE-SEM images of NiV-LDH(Vo) revealing sheet like structure was retained even after vacancy creation through the NaBH₄ reduction under hydrothermal condition and (c) EDS spectrum obtained in FE-SEM mode.

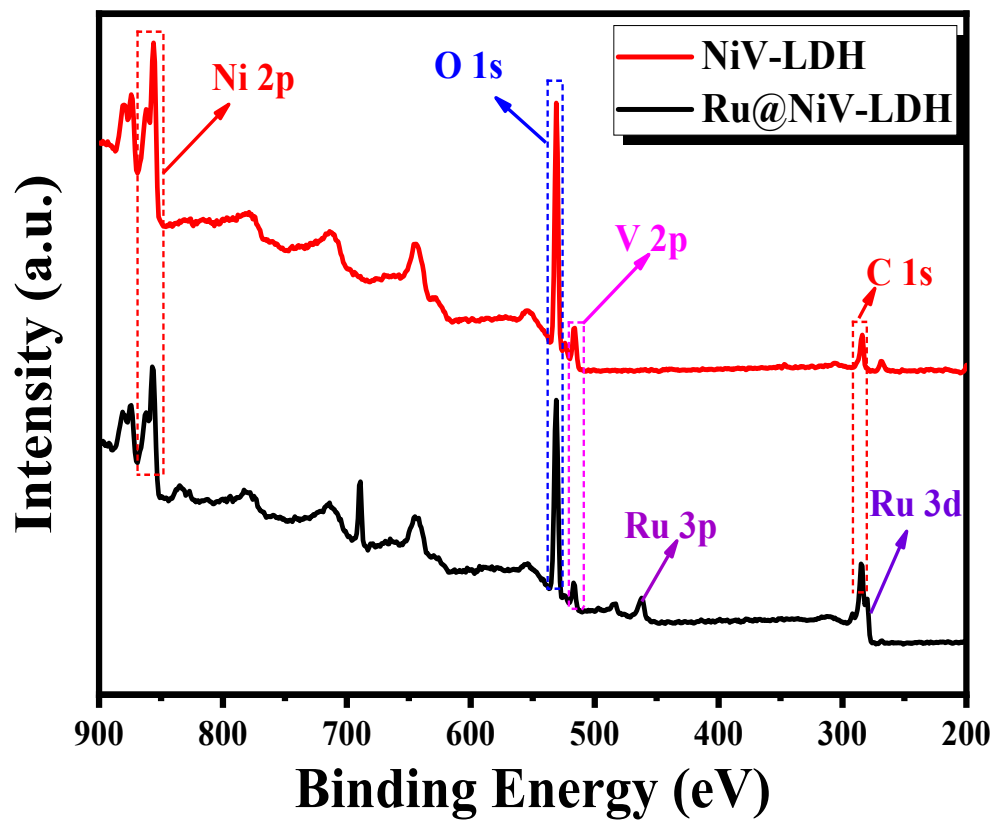


Figure S6: Combined XPS survey spectrum of NiV-LDH and Ru@NiV-LDH.

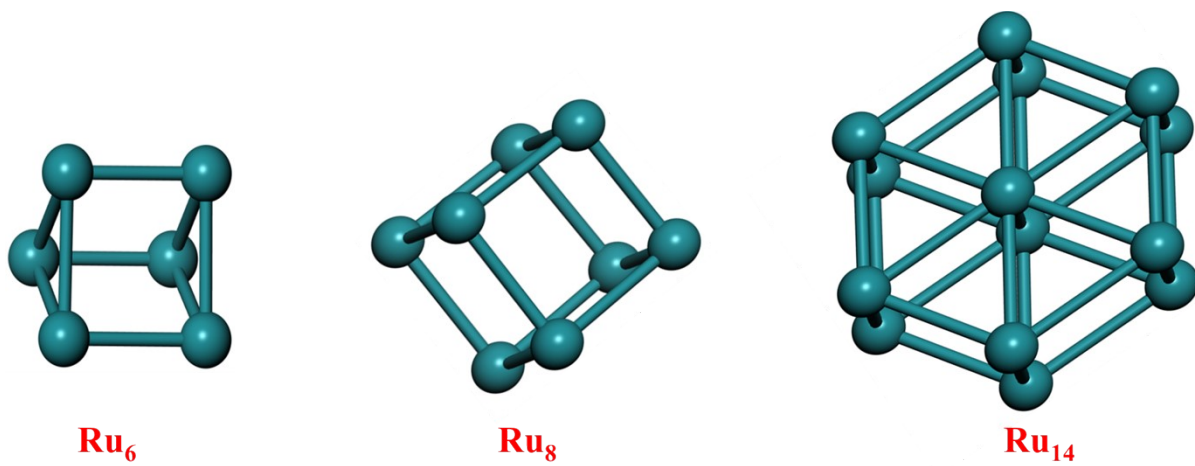


Figure S7: DFT optimized structure of Ru_6 , Ru_8 and Ru_{14} clusters.

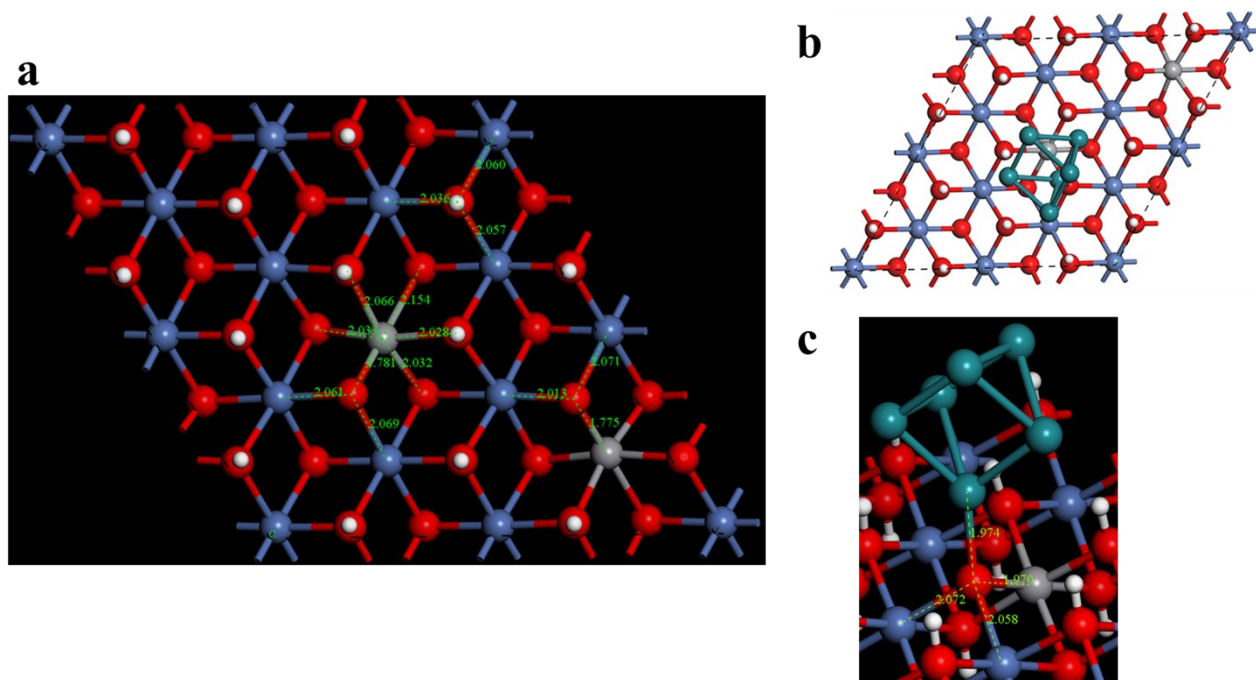


Figure S8: (a) Ball and stick model of optimized structure of monolayer of $\text{Ni}_{5/6}\text{V}_{1/6}(\text{OH})_2$ compound (top view); (b) Ru_6 cluster deposited on $\text{Ni}_{5/6}\text{V}_{1/6}(\text{OH})_2$ compound, and (c) closer view of (b) to understand bonding between O-Ru atoms. Blue, light grey, red, turquoise blue and white balls represent Ni, V, O, Ru and H atoms, respectively. Dotted black line indicates boundary of supercell. Bond distances are shown in Å.

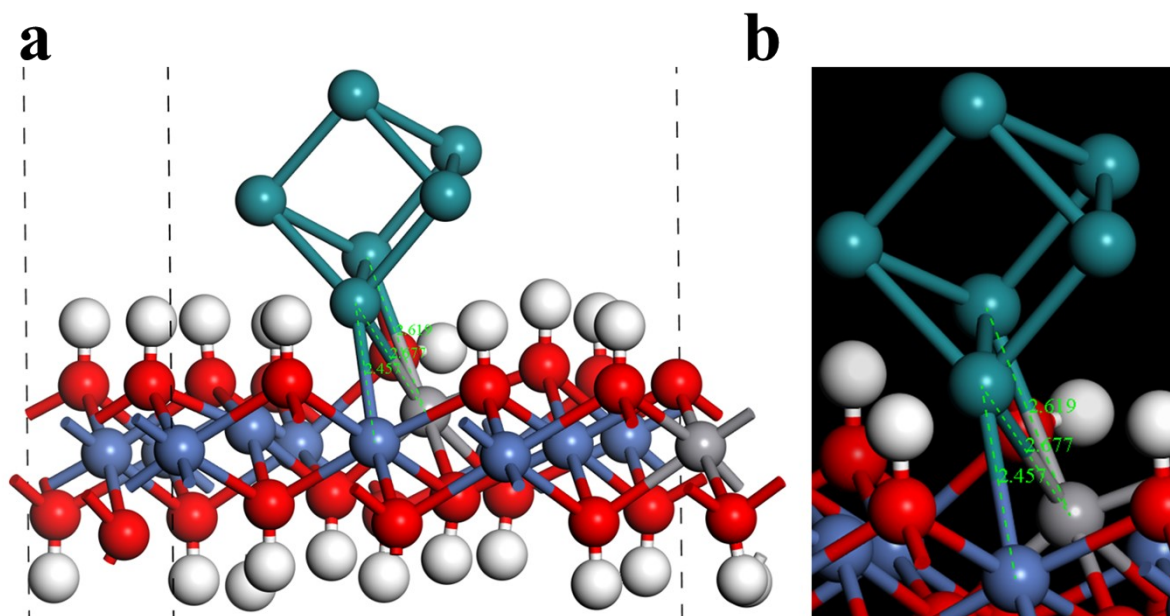


Figure S9: (a) Optimized structure of Ru₆ cluster adsorbed on oxygen deficient surface (b) closer view of the cluster and surface. Blue, light grey, red, turquoise blue and white balls represent Ni, V, O, Ru and H atoms, respectively. Dotted line indicates boundary of supercell. Bond distances are shown in Å.

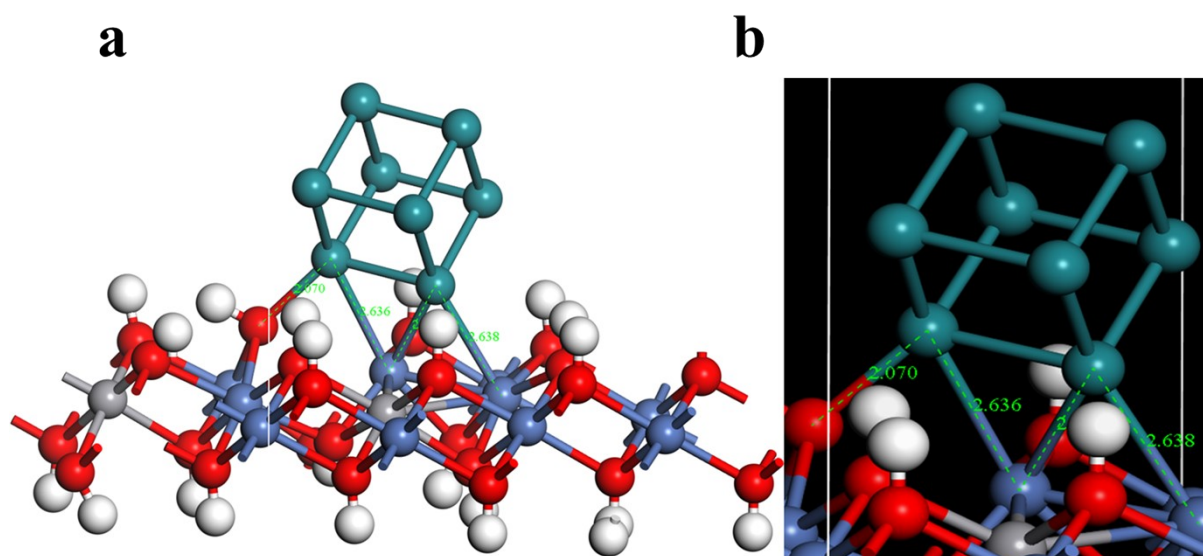


Figure S10: (a) Optimized structure of Ru₆ cluster adsorbed on oxygen deficient surface (b) closer view of the cluster and surface. Blue, light grey, red, turquoise blue and white balls represent Ni, V, O, Ru and H atoms, respectively. Dotted line indicates boundary of supercell. Bond distances are shown in Å.

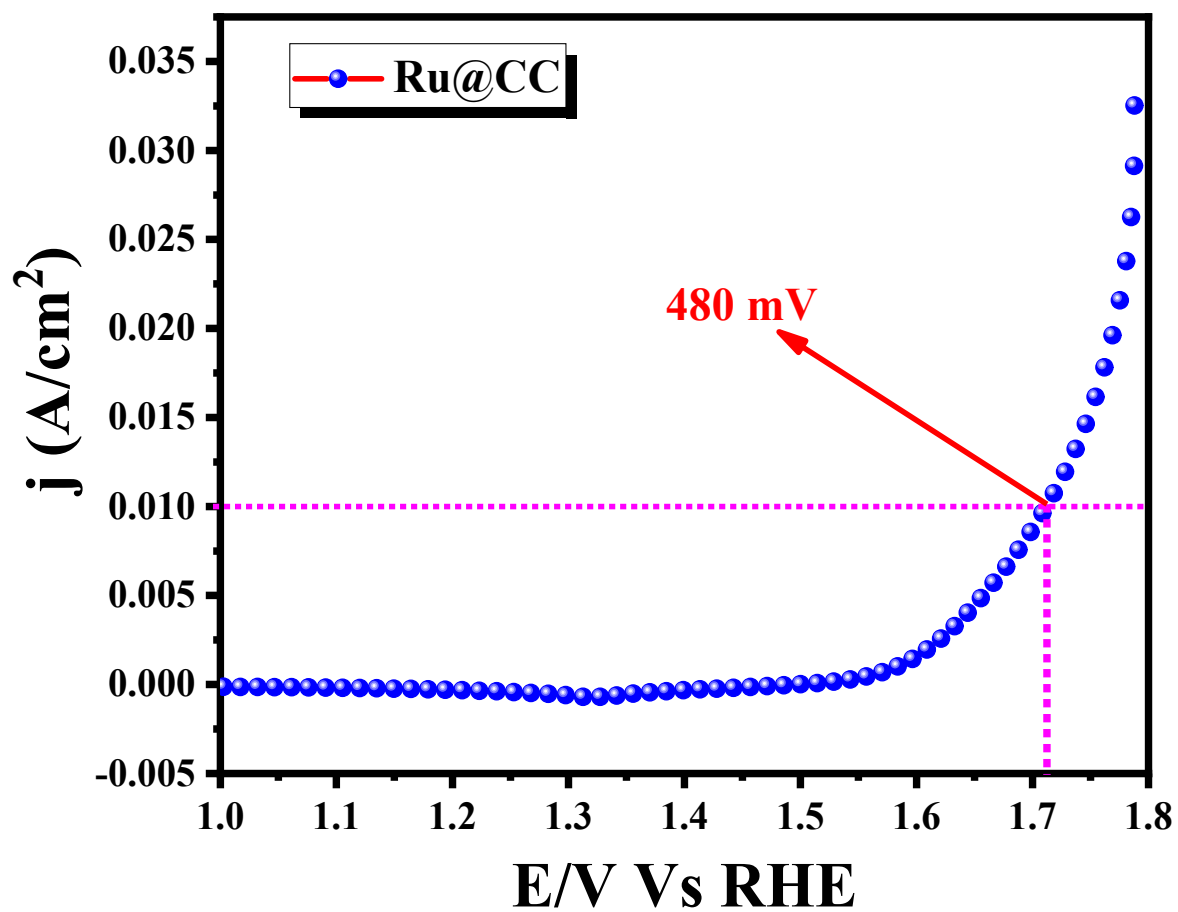


Figure S11: LSV polarization curve for Ru@CC obtained at a scan rate of 5 mV/sec in 1 M KOH solution.

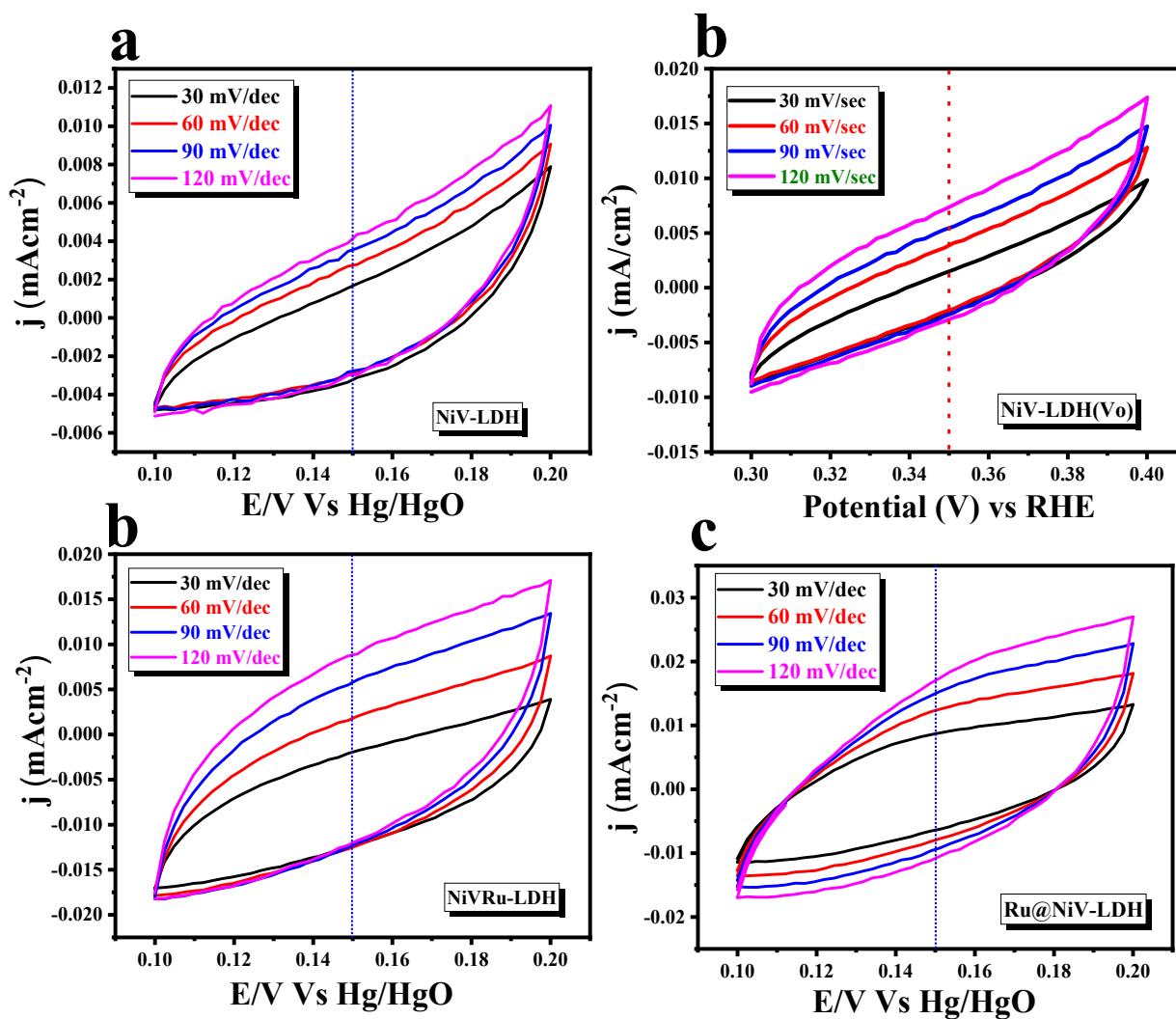


Figure S12: (a-d) are the CVs recorded in a non-faradaic region with increasing scan rate for the determination of ECSA from its double layer capacitance taking NiV-LDH, NiV-LDH(V_o), NiVRu-LDH and Ru@NiV-LDH respectively.

| Sl. No. | Catalysts | Overpotential (mV) | Tafel Slope (mV/dec) | Ref. |
|-----------|--|---------------------------------|----------------------|------------------|
| 1 | Co ₂ (OH) ₃ Cl/vanadium oxide | 282@ 10 mA/cm ² | 56 | 3 |
| 2 | Co-V Hydroxide Nanoneedle | 268@ 10mA/cm ² | 80 | 4 |
| 3 | a-CoVO _x | 347@ 10 mA/cm ² | 35 | 5 |
| 4 | wrinkled Ni(OH) ₂ | 358.2@ 10mA/cm ² | 54.4 | 6 |
| 5 | Cobalt–Iron–Vanadium Layered Double Hydroxide | 242@ 10mA/cm ² | 57 | 7 |
| 6 | Ni(OH) ₂ | 437@ 10mA/cm ² | 127 | 8 |
| 7 | NiO _x | 331@ 10mA/cm ² | 47 | 9 |
| 8 | 3D CeO ₂ /Ni(OH) ₂ /carbon foam | >350@ 10mA/cm ² | 57 | 10 |
| 9 | FeOOH on Ni(OH) ₂ | 245@ 50mA/cm ² | 45 | 11 |
| 10 | NiV-LDH@FeOOH | 297@ 100mA/cm ² | 57.3 | 12 |
| 11 | VO(OH) ₂ nanosheets grown on NiFe LDH nanoflowers | 280@ 100mA/cm ² | 65 | 13 |
| 12 | Nickel–vanadium monolayer double hydroxide | >300@ 10mA/cm ² | 50 | 14 |
| 13 | V-doped CoP nanoparticles | 340@ 10mA/cm ² | - | 15 |
| 14 | Ru@NiV-LDH | 272@ 10mA/cm² | 40 | This work |

Table S1: Comparison study of the electrocatalytic performance of synthesized Ru@NiV-LDH catalyst compared to similar types of catalysts.

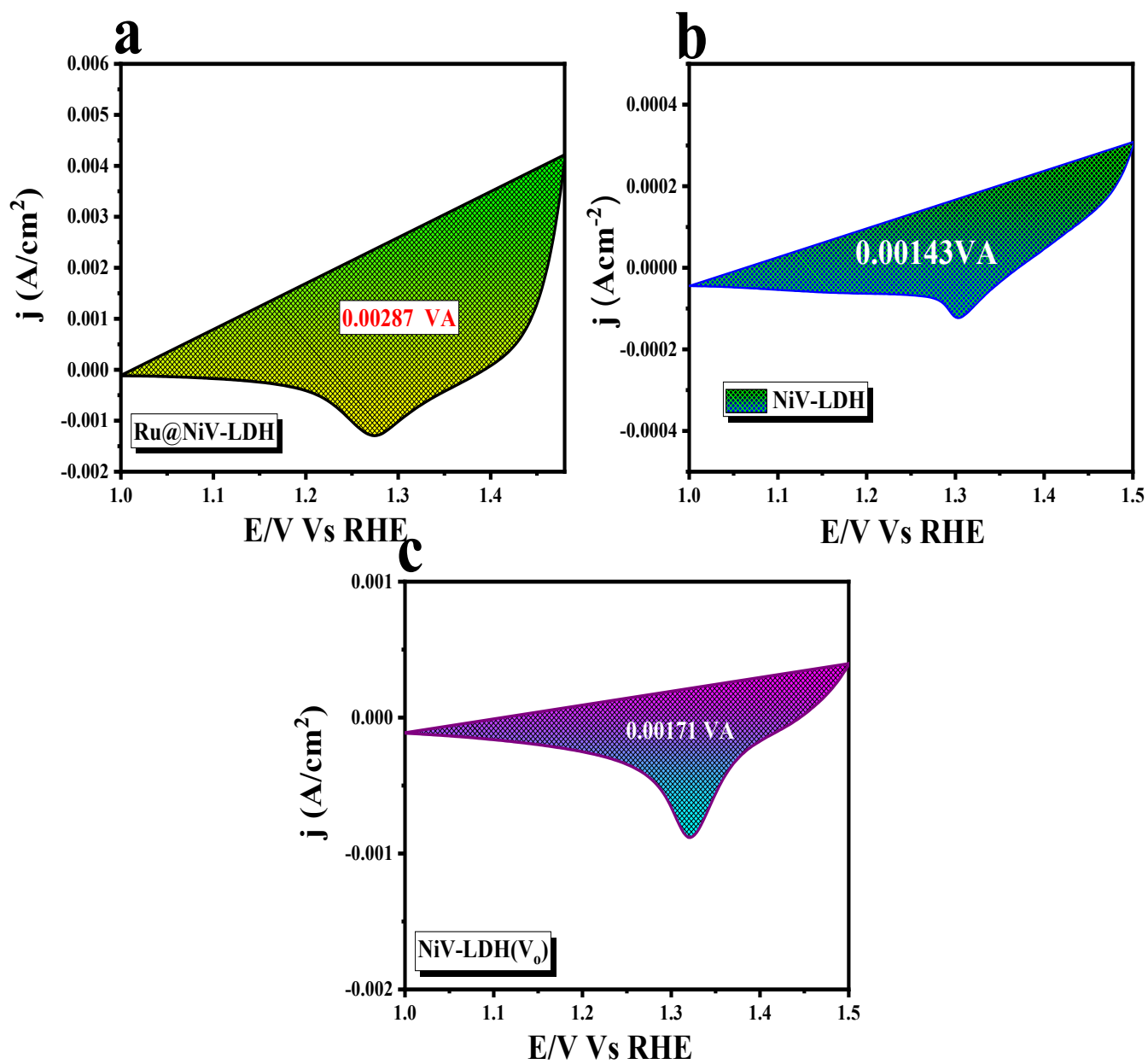


Figure S13: (a), (b) and (c) Reduction surface area of Ru@NiV-LDH, NiV-LDH and NiV-LDH (V_o) respectively.

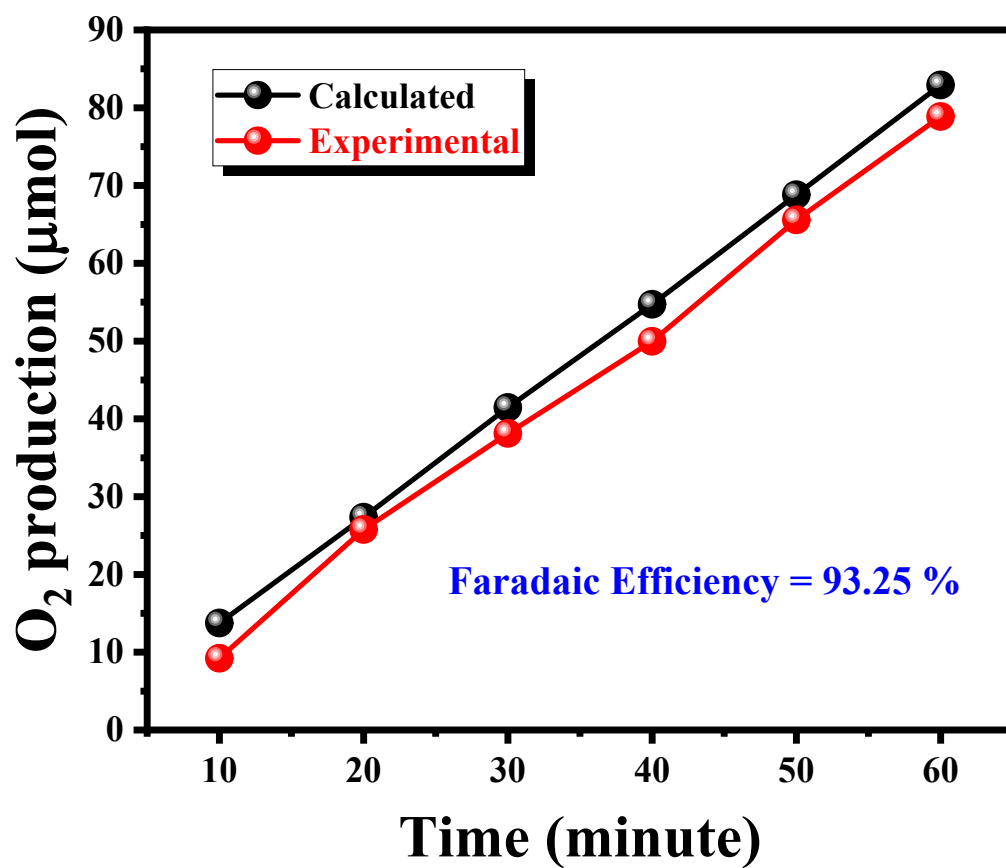


Figure S14: Faradaic efficiency plot obtained by plotting the amount of O₂ produced at different time interval.

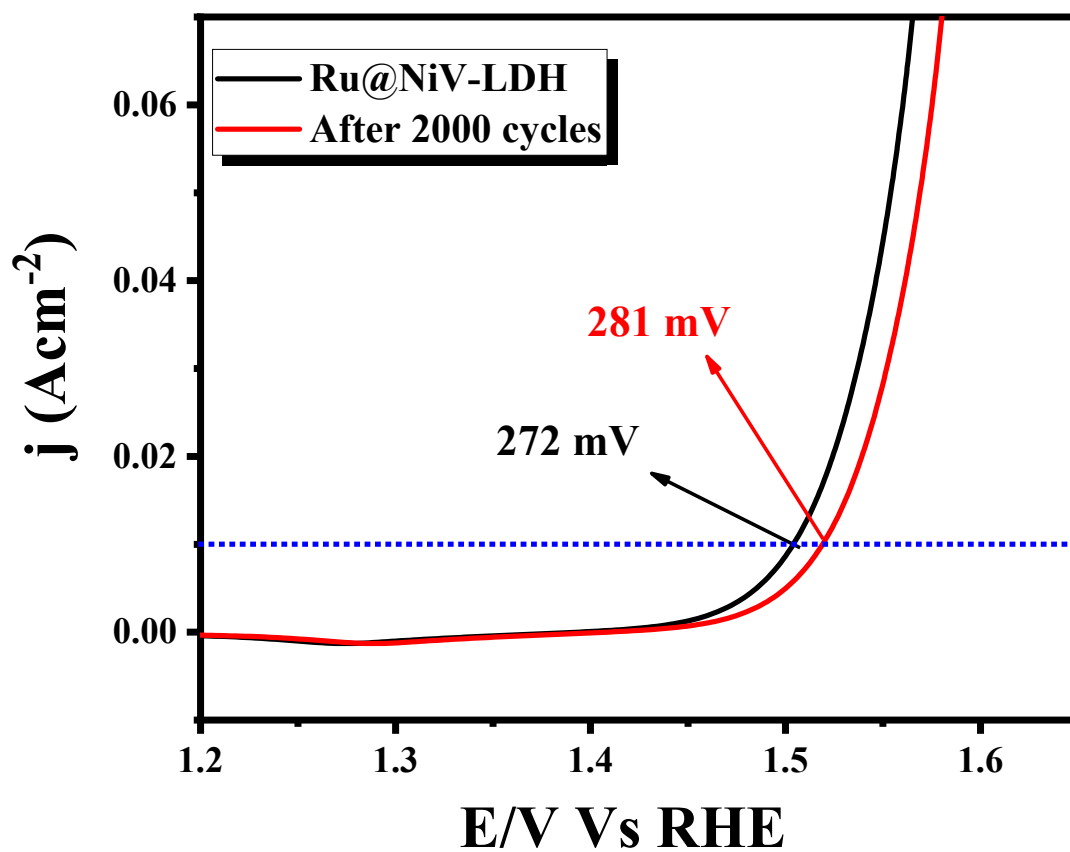


Figure S15: LSV polarization curves for Ru@NiV-LDH materials before and after the AD study.

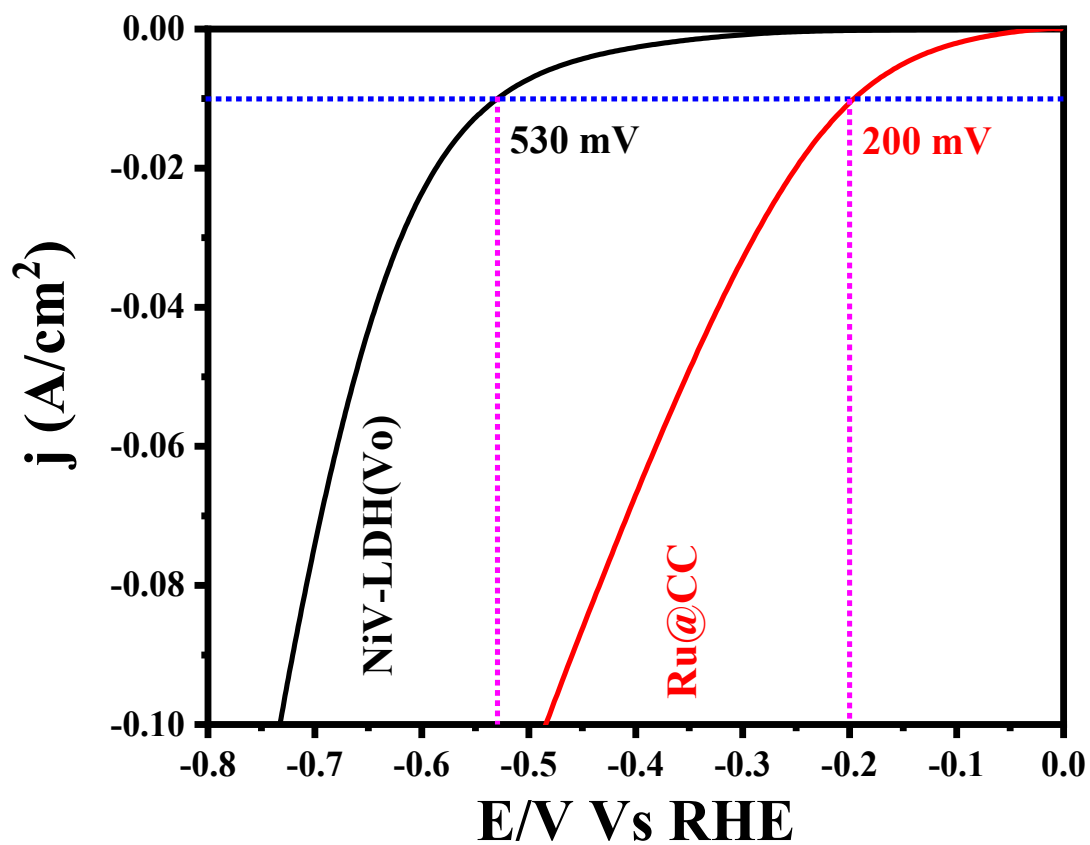


Figure S16: LSV polarization curves of NiV-LDH(Vo) and Ru@CC under HER condition.

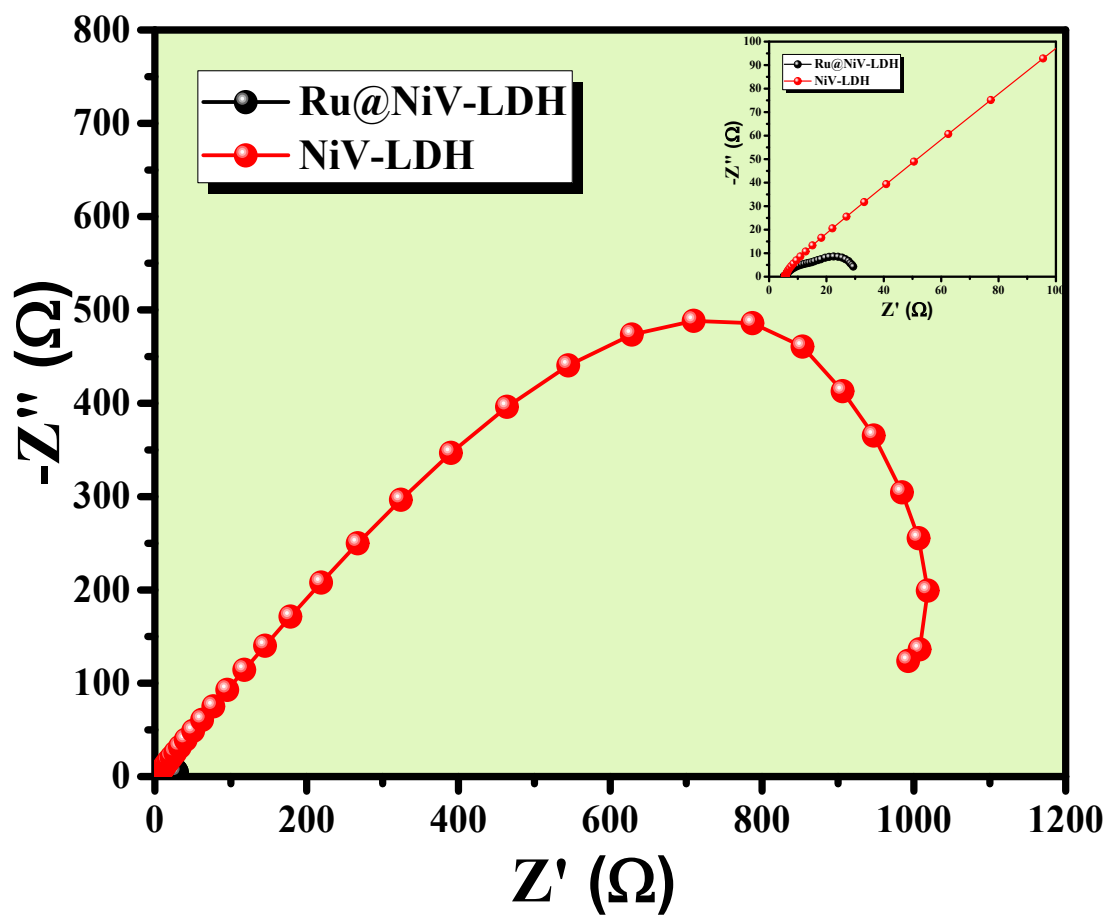


Figure S17: EIS analysis of NiV-LDH and Ru@NiV-LDH in HER condition.

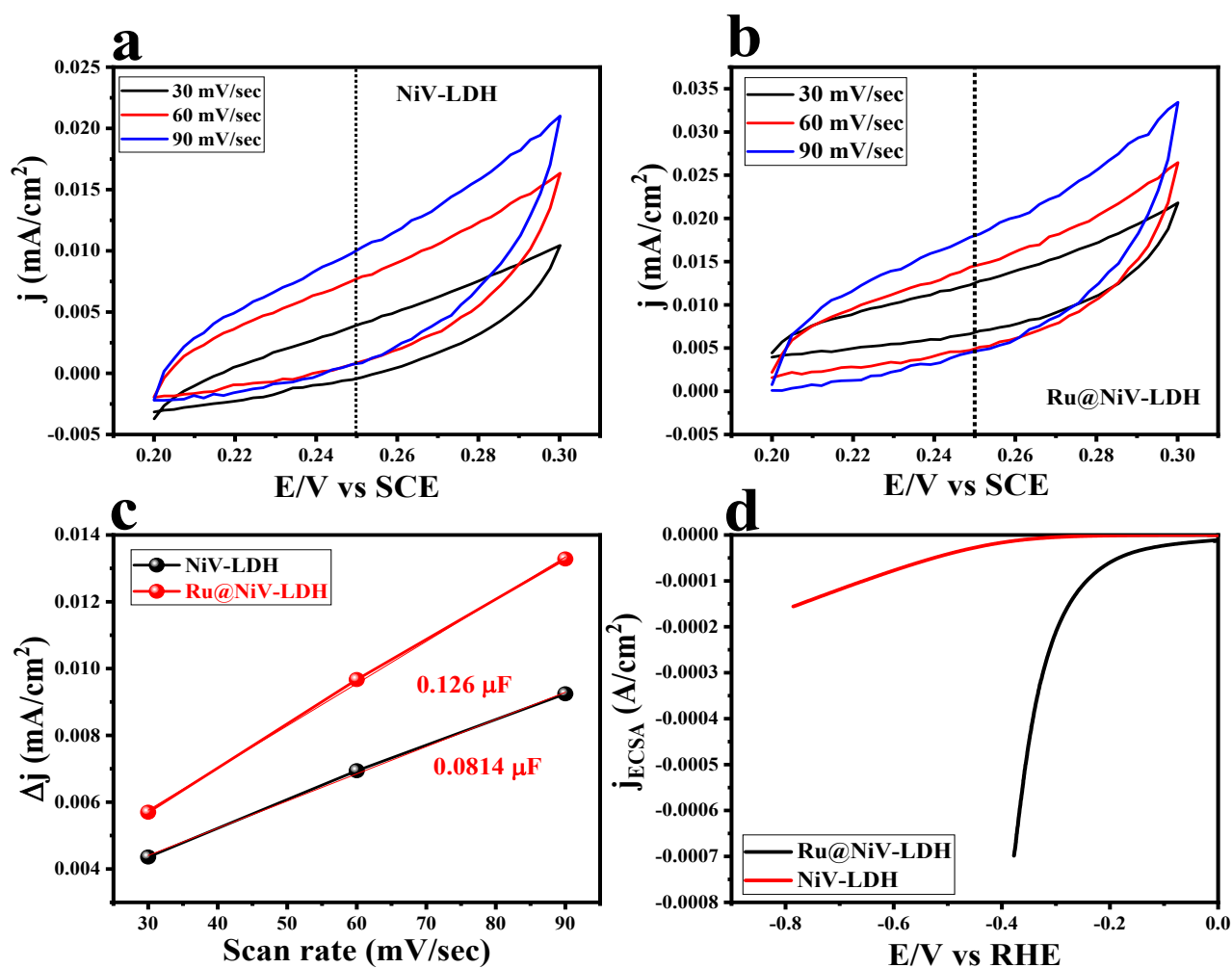


Figure S18: (a-b) CV curves obtained at different scan rate for NiV-LDH and Ru@NiV-LDH respectively; (c) corresponding C_{dl} plot and (d) ECSA normalized LSV polarization curves.

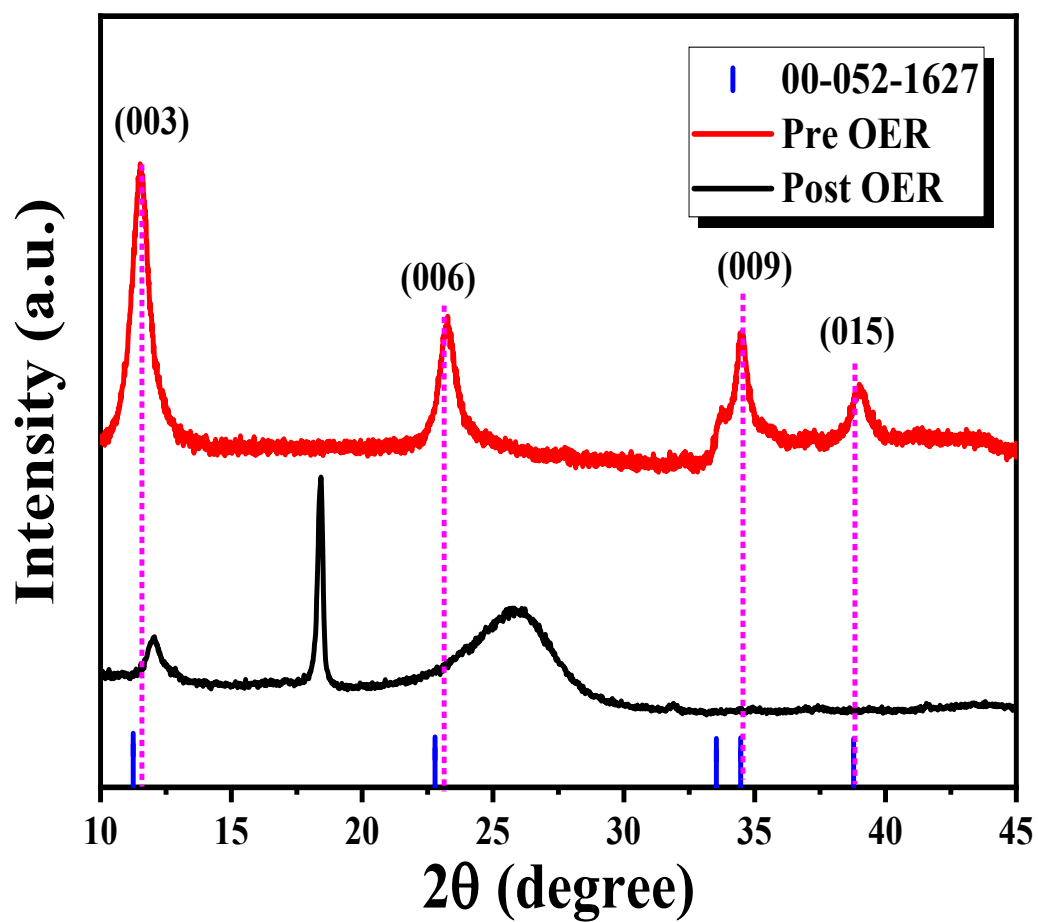


Figure S19: XRD pattern of Ru@NiV-LDH before and after the electrolysis.

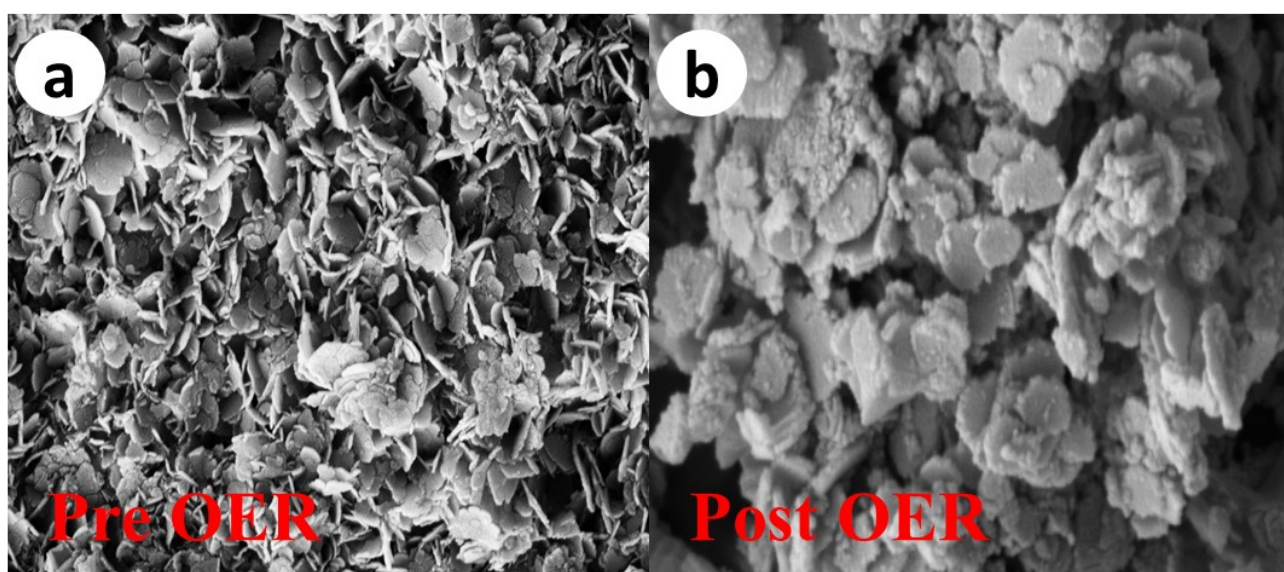


Figure S20: Pre and post OER, FE-SEM picture of Ru@NiV-LDH.

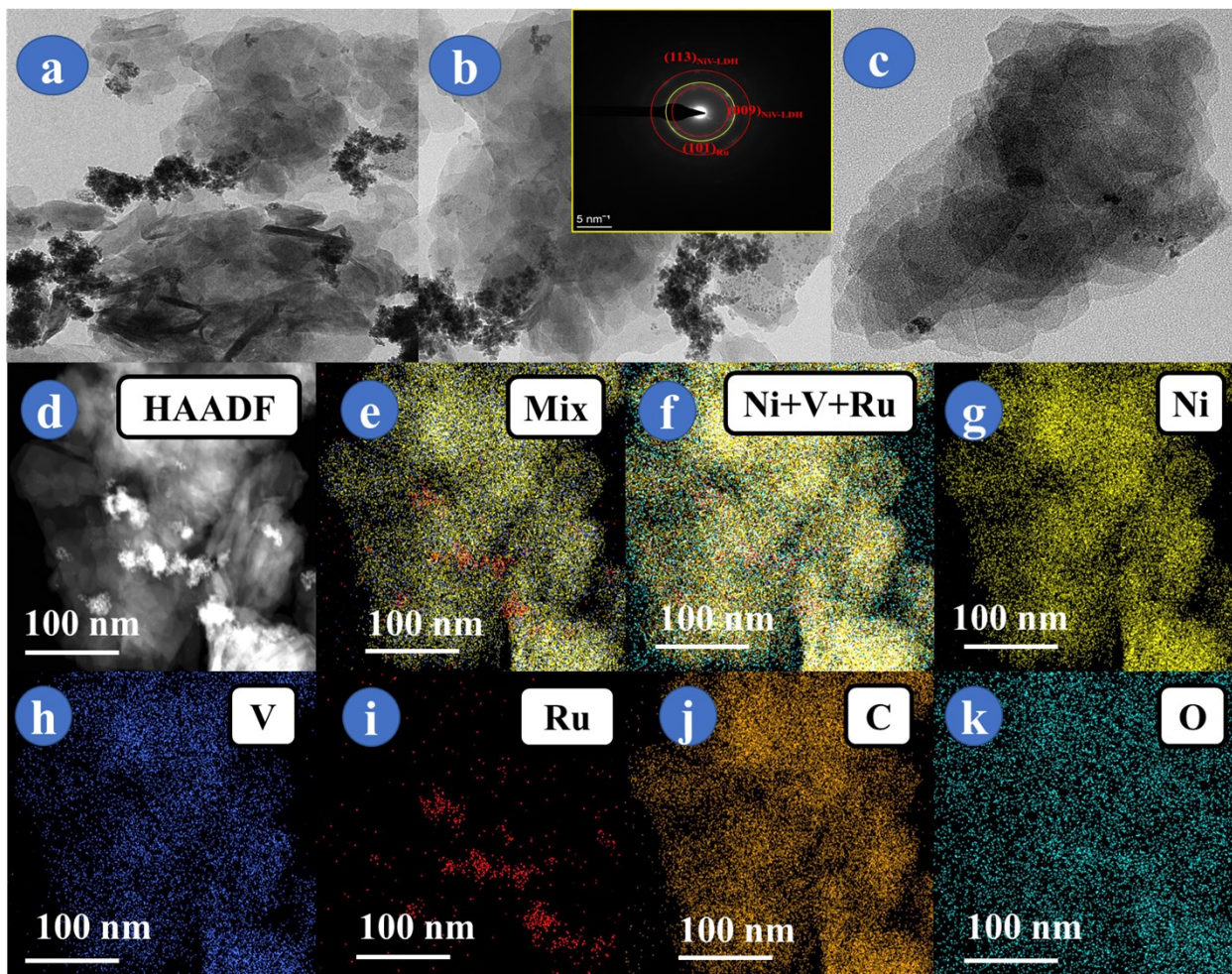


Figure S21: (a-c) Low to high magnified Post OER HR-TEM images of Ru@NiV-LDH nanosheets; (d) HAADF area chosen for colour mapping and (e-k) showing the colour mapping results of HAADF+Ni+V, mix, Ni K shell, V K shell, O K shell and C K shell orbitals respectively.

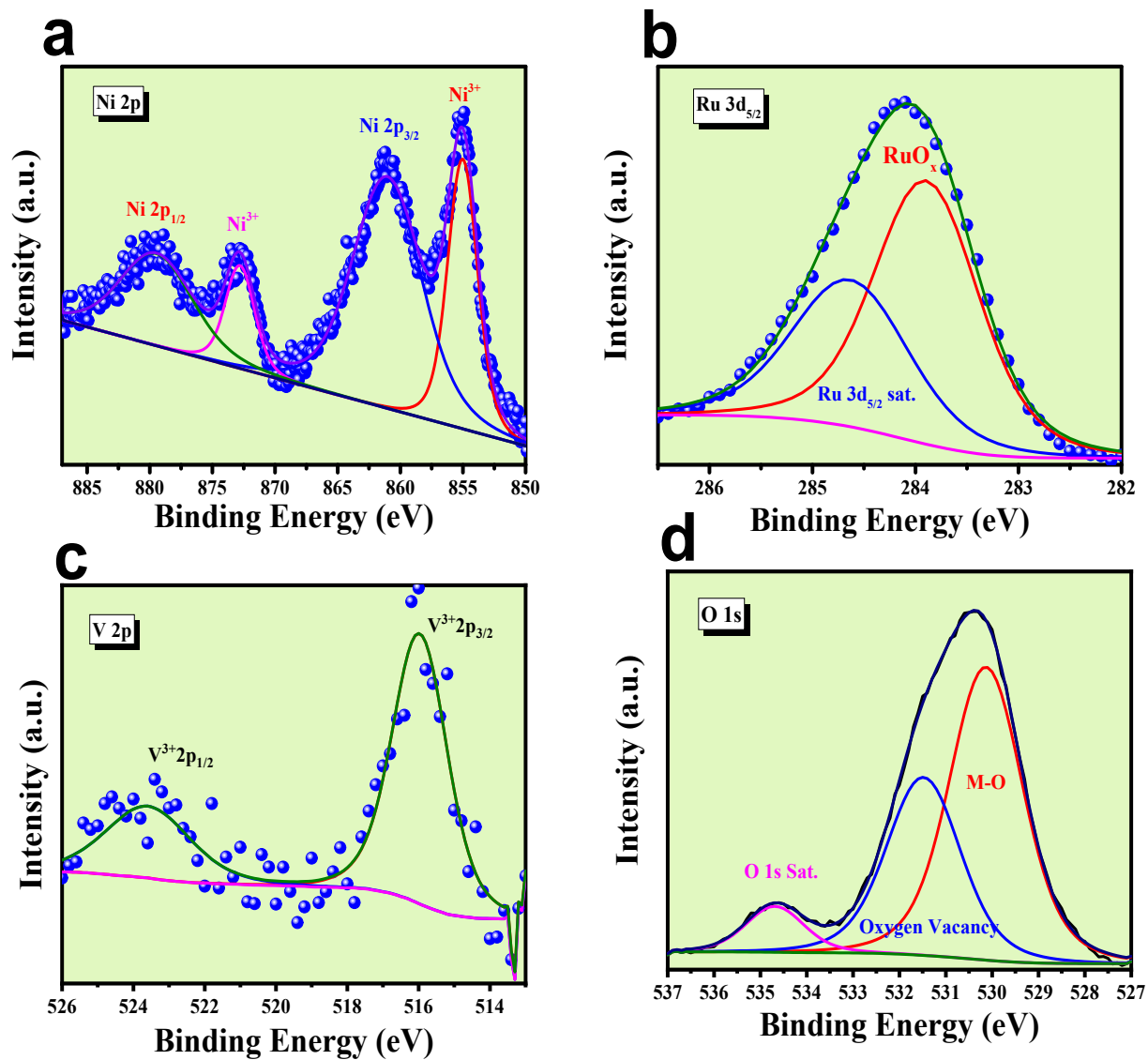


Figure S22: (a) High resolution XPS spectra of Ni 2p orbitals post OER Ru@NiV-LDH respectively; (b) Ru 3d XPS result; (c) High resolution XPS spectra of V 2p orbital; (d) O 1s orbital XPS spectra.

References

- 1 N. Holzwarth, G. Matthews, R. Dunning, A. Tackett and Y. Zeng, *Phys. Rev. B - Condens. Matter Mater. Phys.*, 1997, **55**, 2005–2017.
- 2 J. P. Perdew, K. Burke and M. Ernzerhof, *Phys. Rev. Lett.*, 1996, **77**, 3865–3868.
- 3 K. Fan, H. Zou, L. Duan and L. Sun, *Adv. Energy Mater.*, 2020, **10**, 1–9.
- 4 M. Yang, X. Fu, M. Shao, Z. Wang, L. Cao, S. Gu, M. Li, H. Cheng, Y. Li, H. Pan and Z. Lu, *ChemElectroChem*, 2019, **6**, 2050–2055.
- 5 L. Liardet and X. Hu, *ACS Catal.*, 2018, **8**, 644–650.
- 6 Y. Dou, L. Zhang, J. Xu, C. T. He, X. Xu, Z. Sun, T. Liao, B. Nagy, P. Liu and S. X. Dou, *ACS Nano*, 2018, **12**, 1878–1886.
- 7 Y. Hu, Z. Wang, W. Liu, L. Xu, M. Guan, Y. Huang, Y. Zhao, J. Bao and H. M. Li, *ACS Sustain. Chem. Eng.*, 2019, **7**, 16828–16834.
- 8 G. Zhao, P. Li, N. Cheng, S. X. Dou and W. Sun, *Adv. Mater.*, 2020, **32**, 1–9.
- 9 L. A. Stern and X. Hu, *Faraday Discuss.*, 2014, **176**, 363–379.
- 10 Z. Liu, N. Li, H. Zhao, Y. Zhang, Y. Huang, Z. Yin and Y. Du, *Chem. Sci.*, 2017, **8**, 3211–3217.
- 11 W. Guo, D. Li, D. Zhong, S. Chen, G. Hao, G. Liu, J. Li and Q. Zhao, *Nanoscale*, 2020, **12**, 983–990.
- 12 W. Bao, L. Xiao, J. Zhang, Z. Deng, C. Yang, T. Ai and X. Wei, *Chem. Commun.*, 2020, **56**, 9360–9363.
- 13 J. Tang, X. Jiang, L. Tang, Y. Li, Q. Zheng, Y. Huo and D. Lin, *Dalt. Trans.*, 2021, **50**, 1053–1059.
- 14 K. Fan, H. Chen, Y. Ji, H. Huang, P. M. Claesson, Q. Daniel, B. Philippe, H. Rensmo, F. Li, Y. Luo and L. Sun, *Nat. Commun.*, 2016, **7**, 1–9.
- 15 J. F. Qin, J. H. Lin, T. S. Chen, D. P. Liu, J. Y. Xie, B. Y. Guo, L. Wang, Y. M. Chai and B. Dong, *J. Energy Chem.*, 2019, **39**, 182–187.